Available online at www.sciencedirect.com

SciVerse ScienceDirect

Acta Materialia 61 (2013) 5768–5778

Acta MATERIALIA

www.elsevier.com/locate/actamat

The evolved microstructure ahead of an arrested fatigue crack in Haynes 230

D.W. Gross [a], K. Nygren [a], G.J. Pataky [b], J. Kacher [a], H. Sehitoglu [b], I.M. Robertson [a,b,*]

[a] Department of Materials Science and Engineering, University of Illinois, Urbana, IL, USA
[b] Department of Mechanical Science and Engineering, University of Illinois, Urbana, IL, USA

Received 26 February 2013; received in revised form 27 April 2013; accepted 12 June 2013
Available online 9 July 2013

Abstract

The dislocation microstructure beneath surface slip traces produced by fatigue loading of Haynes 230 was revealed to be a function of distance from a crack tip. The microstructure beneath these traces evolves from planar slip bands with increasing dislocation density and decreasing interband spacing as the crack tip approaches one of refined subgrains and lamellar bands at and in the vicinity of the crack tip. Similarly, beneath fatigue striations the microstructure evolves from nanosized subgrains to a banded structure with increasing distance from the fracture surface. These structures are significantly different to those predicted to develop under fatigue loading of a planar slip material. The evolved structures are considered in terms of the microstructure generated by severe plastic deformation.

Keywords: Electron microscopy; Fatigue; Microstructure

1. Introduction

Understanding the evolution of the dislocation microstructure and strain localization as a function of cyclic loading is central to determining fatigue crack initiation [1–4]. As current understanding of the evolution processes have been reviewed extensively, only the salient features for face-centered cubic (fcc) systems are mentioned briefly [2,4–9]. The cyclic stress–strain curves of pure fcc single crystal metals exhibit a common form that can be divided into three regions. The first, at low plastic strain amplitudes, is characterized by work hardening, which is attributed to the interaction between primary dislocation dipoles. These dipoles accumulate in regions, patches, which themselves amass and intersect to form a vein structure. At this stage, the strain is carried by the dislocation loops in the patches and in the channels between them by Taylor lattice flipping and motion of screw dislocations, respectively. Correspondingly, the slip markings on the surface are long, straight and distributed homogeneously. At the onset of the second stage, the plateau stage, these patches occupy about 50% of the volume. Within the plateau region, the microstructure transitions from veins to persistent slip bands. In the third region, saturation, the microstructure evolves from persistent slip bands to a labyrinth and finally to a cell structure. Although this evolution of the microstructure was developed for single crystals, the evolution pathway is relevant to surface grains in large-grained polycrystalline systems. In addition, similar microstructures have been observed in interior grains of some fcc polycrystalline metals. For materials that deform by planar slip, the microstructure evolution is different. At low applied strain amplitudes, the microstructure consists of planar dislocation segments, dipoles and multipoles. At high strain amplitudes, it consists of dislocation tangles and loops. The vein and cell wall structures found in multislip systems are not established. The persistent slip bands are replaced with planar Lüders bands, which like persistent slip bands can create hills and valleys on the exterior surface [10].

* Corresponding author at: Department of Materials Science and Engineering, University of Illinois, Urbana, IL, USA.
E-mail address: irobertson@wisc.edu (I.M. Robertson).

1359-6454/$36.00
http://dx.doi.org/10.1016/j.actamat.2013.06.020

Prior investigations of the microstructure evolution during fatigue loading have relied on extracting samples for examination in the transmission electron microscope by sectioning the sample and cutting a disc from the sectioned slice. Consequently, for the majority of studies the revealed microstructure is several micrometers from the crack tip or from the fracture surface. The interpretation of the results assumes the microstructure to be unaffected by the extraction and preparation processes. The results of these studies show the microstructure increasing in complexity as the crack tip or flank is approached. Within the primary regions of the plastic zone, the microstructure in multislip fcc systems essentially evolves from persistent slip bands mixed with dislocation cells to dislocation cells; the dislocation cell size decreasing as the crack tip or flank is approached. It has been reported that the cell size is inversely proportional to the stress intensity factor [11] or the saturation stress amplitude [12]. In other regions of the plastic zone, the vein structure exists.

In this paper the results of a multiscale investigation of a snapshot in the evolution of the microstructure ahead of a fatigue crack growing in Haynes 230 as a function of distance from the crack tip are presented. Electron backscattering diffraction (EBSD) and digital image correlation (DIC) techniques are employed to determine the evolution at the macroscale in front of the crack tip. Focused ion beam (FIB) machining is used to extract samples normal to the surface from selected regions ahead of the crack tip or from the fracture surface for subsequent examination using a transmission electron microscope. This method provides insight into the dislocation microstructure as a function of distance from the crack tip or fracture surface and has enabled the dislocation structure at the crack tip to be revealed for the first time. The evolved microstructure as a function of distance ahead of the crack is compared and contrasted with that lying beneath striation markings on the fracture surface. A key finding is that the subsurface microstructure is more complex than would be envisioned from a posteriori analysis of the information available on either the sample or fracture surface. The findings have implications for dislocation-based modeling of fatigue microstructure evolution.

2. Materials and methods

The material used in this study was Haynes 230, which is a solid-solution-treated alloy that was prepared in accordance with Aerospace Material Specification AMS 58778B. The yield strength is 390 MPa [13]. Fatigue samples were machined from the plate to dimensions of 50 mm × 9 mm × 2.5 mm with a gauge section width of 4 mm and length of 30 mm. A through-thickness notch was machined into the specimen by using an electric discharge machine with a final notch thickness, as measured from the EBSD map, of approximately 150 μm. The specimens were then mechanically polished, ending with colloidal silica; one side was used for EBSD analysis and the other for DIC. For DIC analysis, a fine layer of black paint was airbrushed onto one side of the specimen to create a speckle pattern. An IMI 202FT digital camera was used to capture images of the speckle pattern during the fatigue crack growth; additional details regarding the experimental procedure associated with DIC measurements can be found in Carroll et al. [14].

The specimens were cyclically loaded in a servohydraulic load frame at an R-ratio = 0.05 and a stress amplitude of $\Delta\sigma = 270$ MPa; one test was carried to failure and the other was arrested after 53,355 cycles. The EBSD analysis was performed using a JEOL 7000F scanning electron microscope operated at 20 keV and using a step size of 1.5 μm. In addition to inverse pole figure (IPF) maps, kernel average misorientation (KAM) maps were generated by calculating the average misorientation between a single pixel and all surrounding first-nearest-neighbor pixels. Misorientations exceeding 5° were excluded from the calculation to avoid grain boundary effects. Sample preparation by FIB machining was performed using either a FEI DB235 SEM-FIB or a FEI Helios 600i SEM-FIB; the extracted sample extended approximately 10×10^{-6} m from the surface. Here it is important to note that although FIB machining does introduce ion damage it has been shown neither to generate high densities of dislocations nor to modify significantly complex dislocation structures [15–19]. Surface image forces may cause rotations of segments of dislocations intersected by the formation of new surfaces but the thickness of the electron-transparent region (>100 nm) as well as the tangled and pinned nature of the dislocation structures will restrict the influence they have on the reported structures. The TEM imaging was performed using a JEOL 2010 LaB_6 operated at 200 keV.

3. Results

Following the production and polishing of the fatigue specimens, EBSD scans were performed on the polished surface to determine the grain size and to provide a baseline for the subsequent measurement of strain using the KAM method. IPF and KAM maps of the specimen before testing are presented in Fig. 1A and B, respectively. The average grain area was 50 μm^2 and 54% of grain boundaries were Σ3 with no preferred grain orientation. The KAM map demonstrates that the polishing has produced a specimen with a clean surface exhibiting a low dislocation density. To confirm the low dislocation density, a sample for examination in the TEM was extracted from the gauge section, away from the notch, by using FIB machining. The resulting microstructure is shown in the bright-field electron micrograph presented in Fig. 2. The dislocation structure consists of planar deformation bands containing a low density of dislocations and is comparable to a sample prepared from the bulk of the material; planar slip is anticipated for this solid-solution-strengthened alloy. This result confirms that the polishing was sufficient to remove all evidence of any case-hardened layer from machining

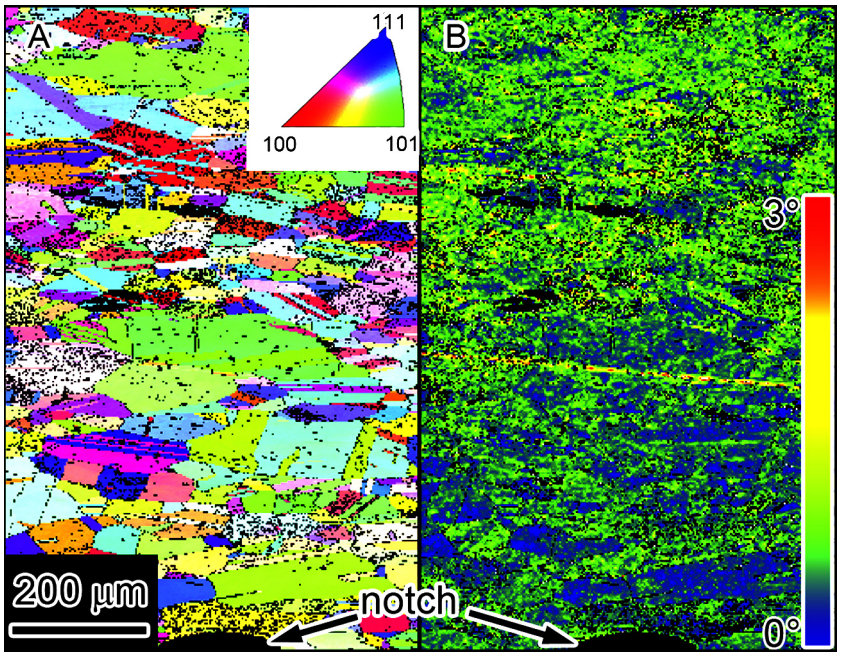

Fig. 1. (A) Inverse pole figure and (B) kernel average misorientation map of the undeformed state. Scan step size was 1.5 μm. (color online).

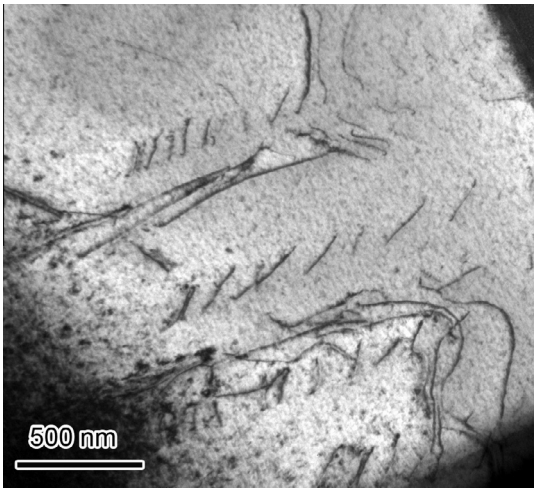

Fig. 2. Initial dislocation microstructure.

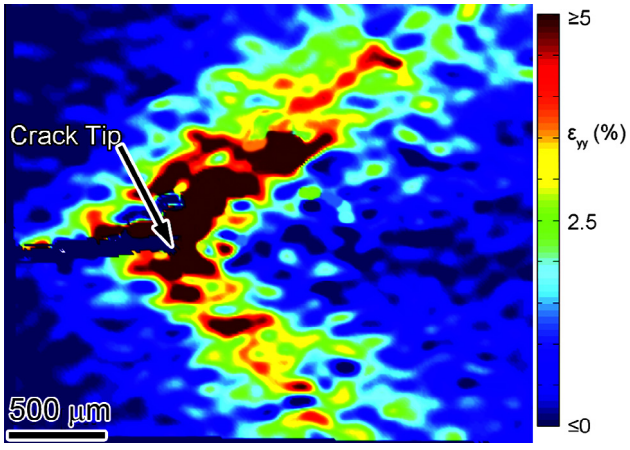

Fig. 3. Results of the DIC strain analysis after 53,000 cycles. (color online).

and that the lift-out process did not introduce a line dislocation structure.

During the fatigue test K_I started at 7 MPa $m^{1/2}$ and increased to 35 MPa $m^{1/2}$ when the crack was arrested. The crack growth as well as the strain evolution was monitored by DIC; detailed analysis of the DIC experiments has been presented elsewhere [14]. A snapshot of the evolved plastic strain after 53,000 cycles is shown in Fig. 3. As demonstrated previously [14], two bands at approximately 45° to the crack growth direction develop, and these two bands do not experience uniform strain as the strain intensity is different in each. The upper branch appears to have experienced a higher and more homogeneous level of strain than the lower branch.

Post-loading EBSD analysis was performed on the surface of the sample to examine the strain in front of the crack tip. This analysis showed an overall increase in strain in front of the crack tip as well as two sharp bands at 45° angles (Fig. 4). However, the non-uniformity of the deformation and strain accumulation within the bands is more apparent than revealed in Fig. 3, and there is evidence for the accumulation of strain at grain boundaries as can be seen by the intense regions that follow the contours of the grain boundaries. This accumulation at the grain boundaries is more obvious in Fig. 4B and C, which are enlargements of the boxed regions in Fig. 4A and in which examples of grain boundaries where strain has accumulated are indicated by arrows.

Prior to examining the underlying microstructure, it is instructive to examine the evolution of the slip traces on

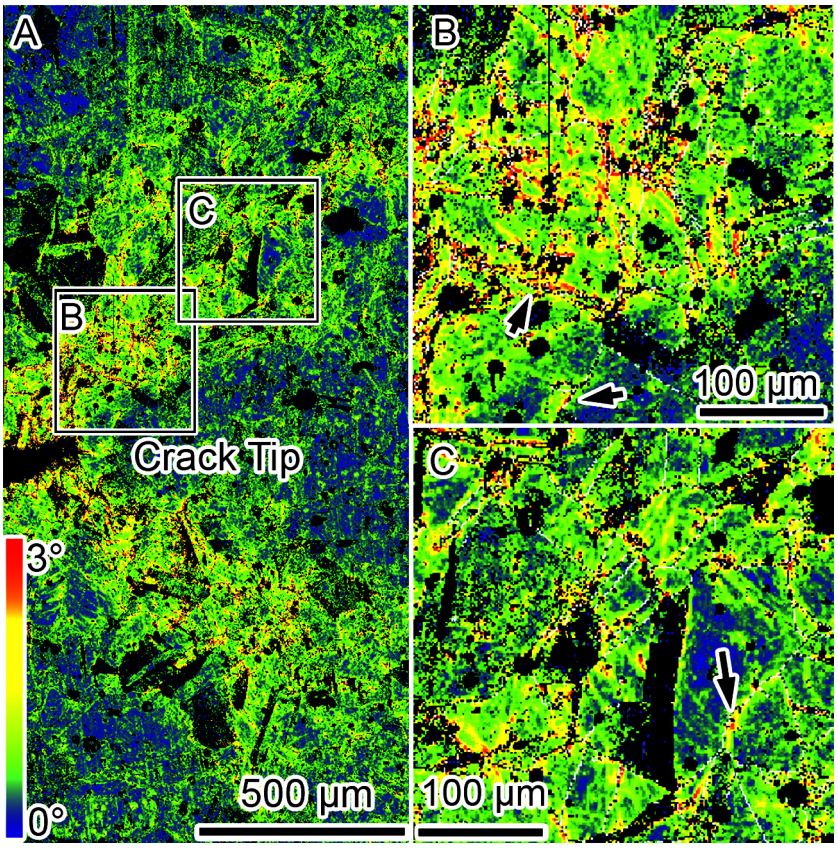

Fig. 4. EBSD map after 53,355 cycles showing the two bands at 45° to the average crack propagation direction. (B, C) Enlarged views of the boxed regions. The scans were done with a step size of 1.5 μm. The arrows indicate grain boundaries at which strain has accumulated. (color online).

the free surface as a function of distance from the crack tip. Furthest from the crack tip, 800 μm, as shown in Fig. 5A the slip traces are long and straight with at least two slip systems active. The distribution of slip is inhomogeneous and regions exhibiting no significant density of slip traces exist. At a distance of about 400 μm, Fig. 5B, the distribution of slip traces becomes more uniform although there is still some irregularity in the spacing between them. The traces remain long and straight, consistent with a low level of plastic strain. At 80 μm from the crack tip, Fig. 5C, the density of slip traces on both visible systems increases and the spacing becomes more regular. Some traces now show evidence of curvature. At the crack tip, Fig. 5D, the intensity of slip traces increases, the trace density is greatest, there is some curvature in some of the lines, and the surface appears buckled and distorted. Although such images, along with the DIC and EBSD analysis, indicate how the accumulated plastic strain varies as a function of distance from the crack tip, they do not provide direct visualization and characterization of the underlying dislocation structures.

Based on the EBSD analysis, eight locations were selected from which samples were extracted using FIB machining for examination by TEM of the subsurface microstructure. As shown in Fig. 6, three locations labeled 1–3 were identified along an arc approximately 800 μm from the crack tip; and these consisted of a position outside the intense strain band, location 1; within the strain band, location 2; and between the two strain bands, location 3; two at locations 4 and 5 approximately 400 μm from the crack tip, inside the strain band and between the strain bands respectively; two locations, 6 and 7, were selected at approximately 80 μm in front of the crack tip and inside the intense strain band; and the final sample was taken directly from the crack tip.

The microstructure beneath each of the eight surface locations is compared and contrasted in Figs. 7–13. The samples extracted from sites approximately 800 μm away from the crack tip exhibited similar microstructures. There is evidence of slip activity on multiple systems and the dislocation density, although greater than in the undeformed material, remains low. Examples of the resulting microstructure are shown in Fig. 7A–C for locations 1–3, respectively. The micrograph from location 2, Fig. 7B, shows the deformation bands are related directly to the slip traces that appear on the surface. The slip trace height reflects the degree of activity on that system. This micrograph also confirms that the surface features are preserved by the platinum strip and are not destroyed by the extraction process or the final thinning to electron transparency.

At a distance of 400 μm, locations 4 and 5, the microstructure looks to be of similar form to that at 800 μm although the density of deformation bands as well as the

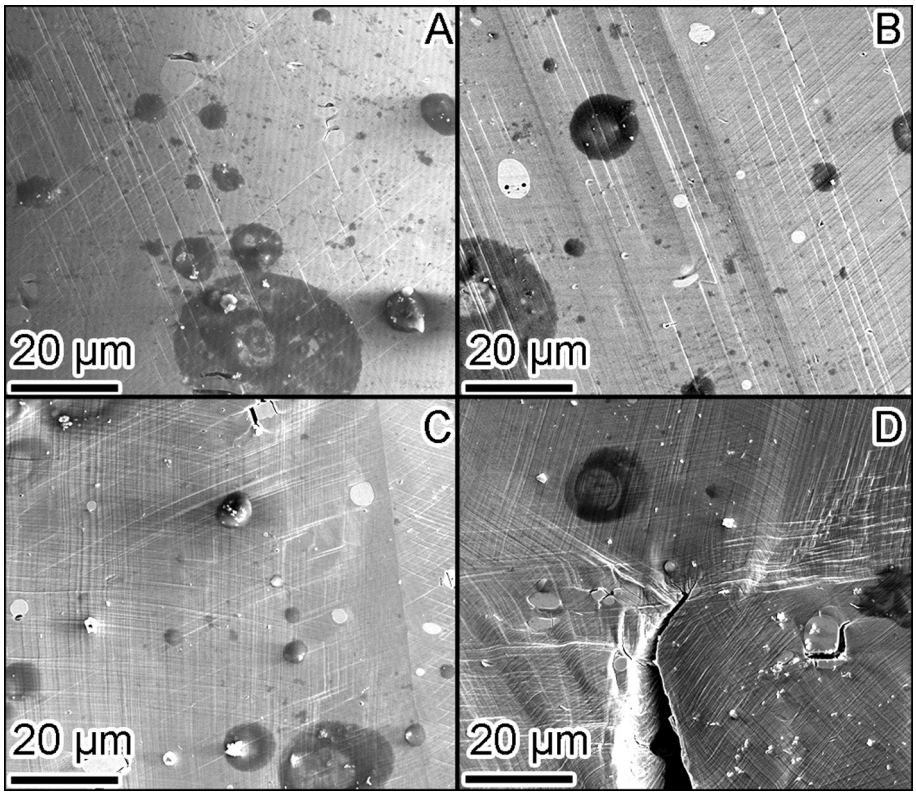

Fig. 5. Comparison of the slip traces on the surface at: (A) 800 μm; (B) 400 μm; (C) 80 μm ahead of the crack tip; and (D) at the crack tip. These locations where used for the subsequent production of FIB liftouts.

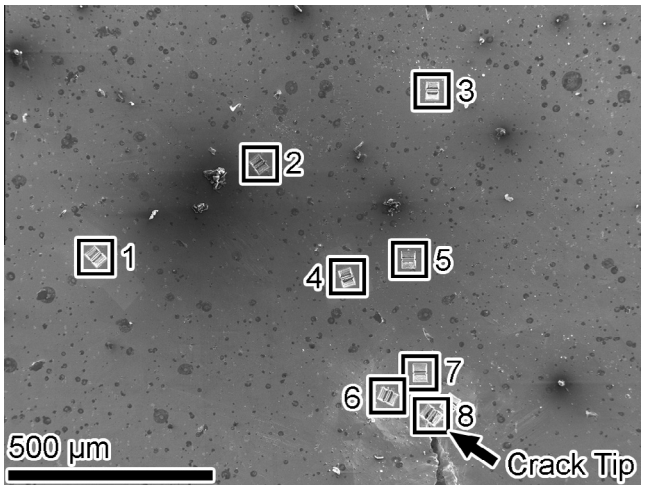

Fig. 6. Identification of the surface locations from which samples were selected. 1–3 are approximately 800 μm, 4 and 5 are 400 μm, 6 and 7 are 80 μm, and 8 captures the crack tip. The bands emerge at approximately 45° to the crack growth direction.

dislocation density within each band has increased. At location 4, Fig. 8A and B, the distance between the bands can be seen to be less and the dislocation density more than in regions at 800 μm. Also, it appears there is significant dislocation activity between the parallel bands, Fig. 9A, but electron tomography reveals this is a projection effect and two distinct sets of parallel bands actually exist. An example of this alignment is shown in views of the electron tomograms from specific vantage directions, Fig. 9B and C. In region 5, the dislocation density is sufficiently low that individual dislocations can be identified and the majority of slip is confined to the bands. The bright-field micrograph shown in Fig. 8D illustrates that in the vicinity of a carbide, the dislocation structure consists of dislocation tangles rather than planar arrays. From a comparison of the microstructures representative of locations 4 and 5, it is clear that the accumulated damage is variable at a distance of 400 μm from the crack tip. This result is consistent with the distribution of slip bands seen at this distance, Fig. 4B.

At 80 μm from the crack tip, the observed microstructure in the two nearby locations shows differences that are immediately and visually apparent. Within the shear band, location 6, the dislocation density has increased to the point where it is difficult to resolve individual dislocations at this magnification, and the distance between each band involving the same slip system has decreased. The bright-field images presented in Fig. 10A and B show examples of this microstructure. In contrast, beneath location 7, Fig. 10C and D, the bands remain poorly defined and contain a low dislocation density that is more comparable to that observed in location 3. These observations reflect the inhomogeneous distribution of the strain even at 80 μm from the crack tip.

The final lift-out captured a portion of the crack tip; this was achieved by covering approximately half of the crack

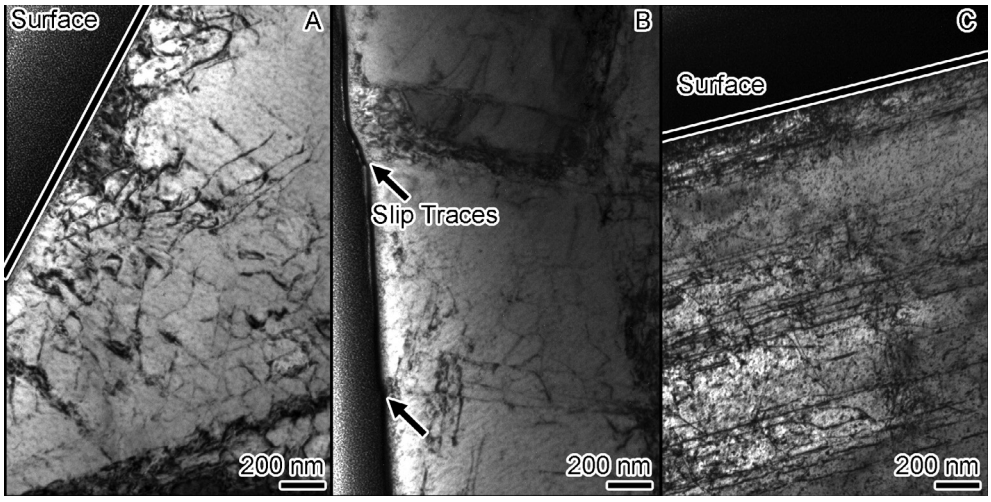

Fig. 7. Bright-field micrographs comparing the microstructure from locations 1–3, which are approximately 800 μm from the crack tip on the free surface.

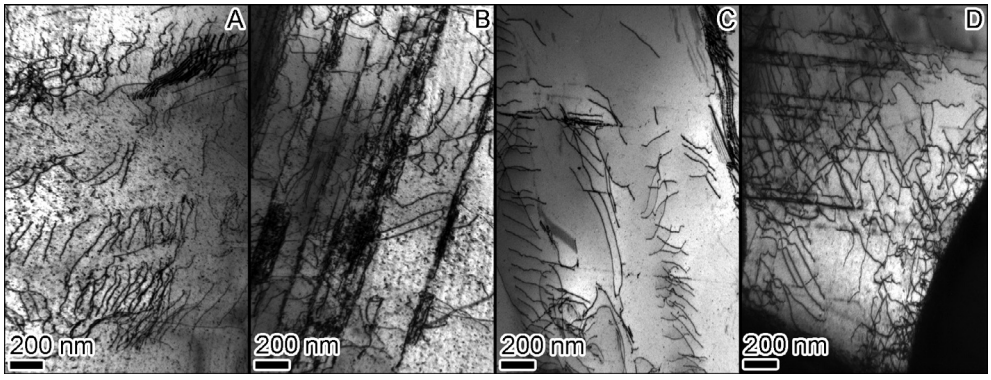

Fig. 8. Comparison of the microstructure from: (A, B) location 4; and (C, D) location 5 at a distance of 400 μm from the crack tip on the free surface.

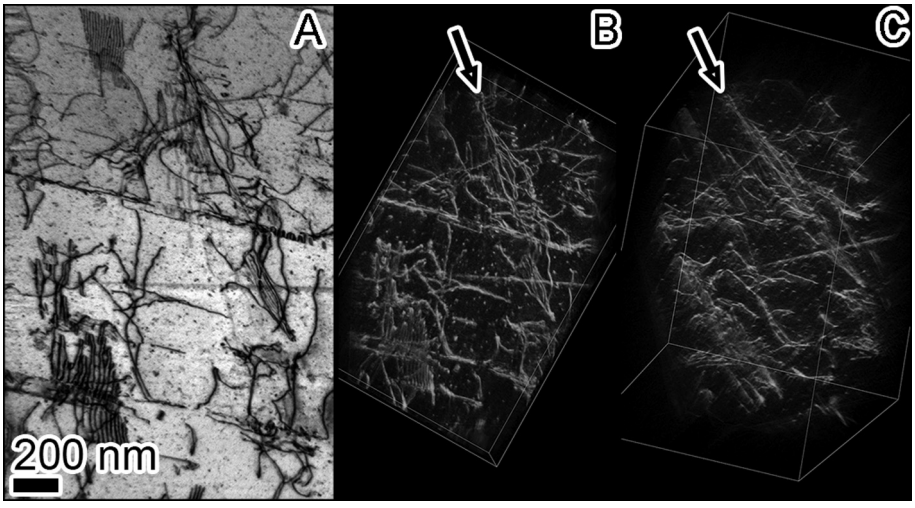

Fig. 9. An area (A) and a tomogram of the same area (B, C) from location 4. The tomogram was acquired over an angular range of 80° with micrographs taken every 1°. The arrows indicate a band of dislocation that may appear to reside between bands in the projected image (A), but collapse into a band when viewed from different vantage directions.

in the direction of crack growth with the platinum strip: the location of the platinum strip with respect to the crack tip is shown in the SEM image presented in Fig. 11A; the direction of crack propagation is also indicated. It is immediately obvious from the traces on the sample surface as well as the distortion that the level of strain this area has

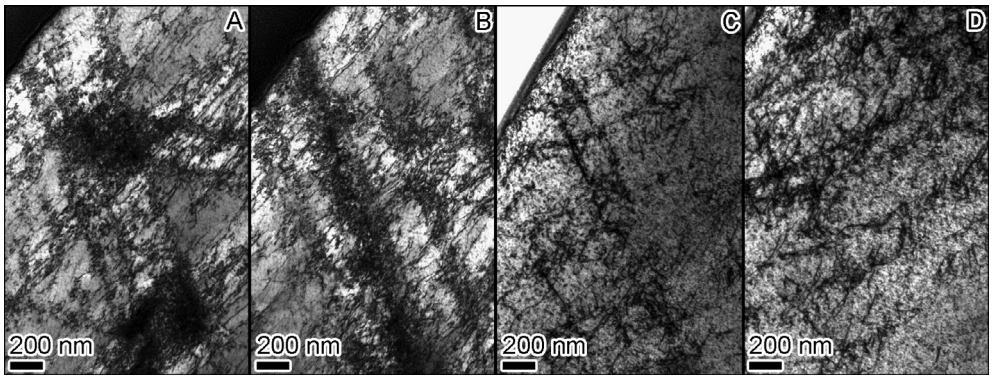

Fig. 10. Comparison of the microstructure from locations at a distance of 80 μm from the crack tip on the free surface. (A, B) are from location 6, and (C, D) are from location 7.

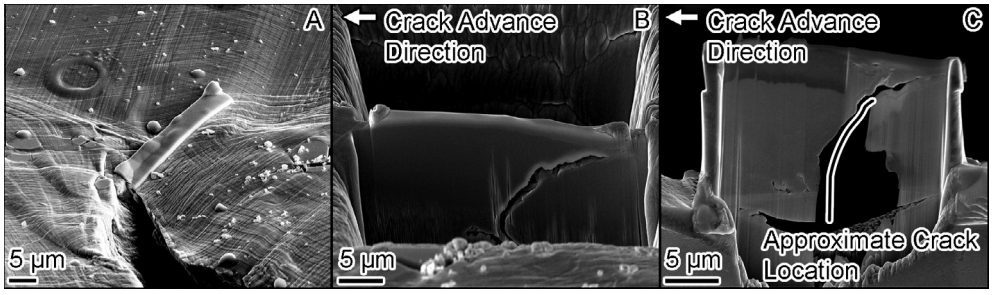

Fig. 11. Stages in the extraction of the sample from the crack tip region. (A) The position of the platinum strip; (B) after the trenches have been machined, the crack tip region is preserved; and (C) loss of material on thinning to electron transparency. The original crack location is indicated by the line.

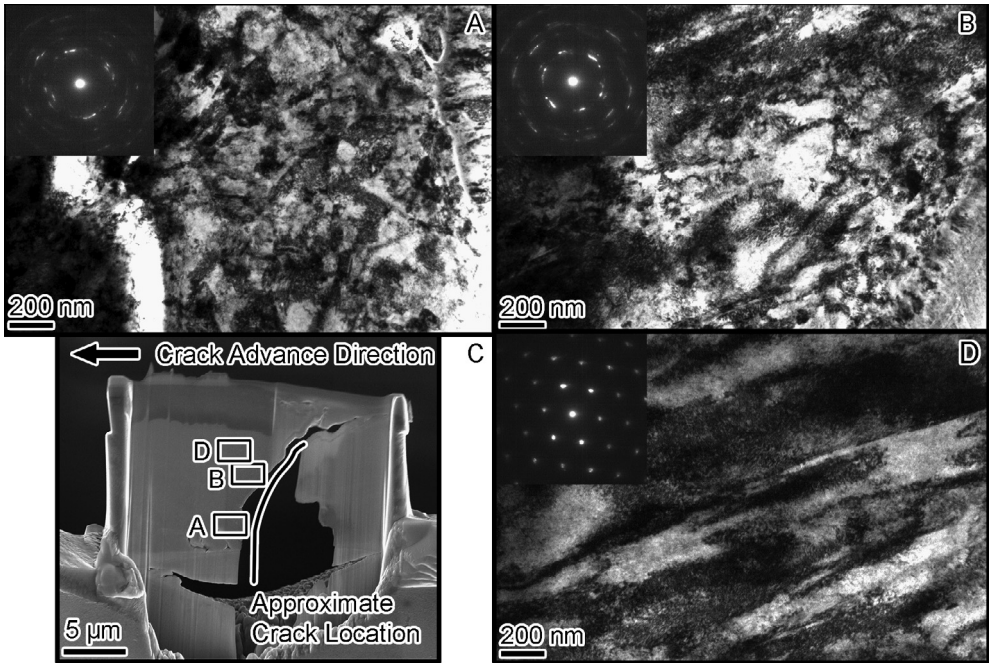

Fig. 12. Microstructure formed in advance of the crack as a function of distance. The approximate locations of the micrographs are shown in (C).

experienced is significantly greater than any of the other regions. The sample preparation process, at least through the initial stages, does not destroy the crack tip region. This can be seen in Fig. 11B, which shows the lift-out after the milling trenches have been created. Here the location of the advancing crack in the interior to that on the surface is

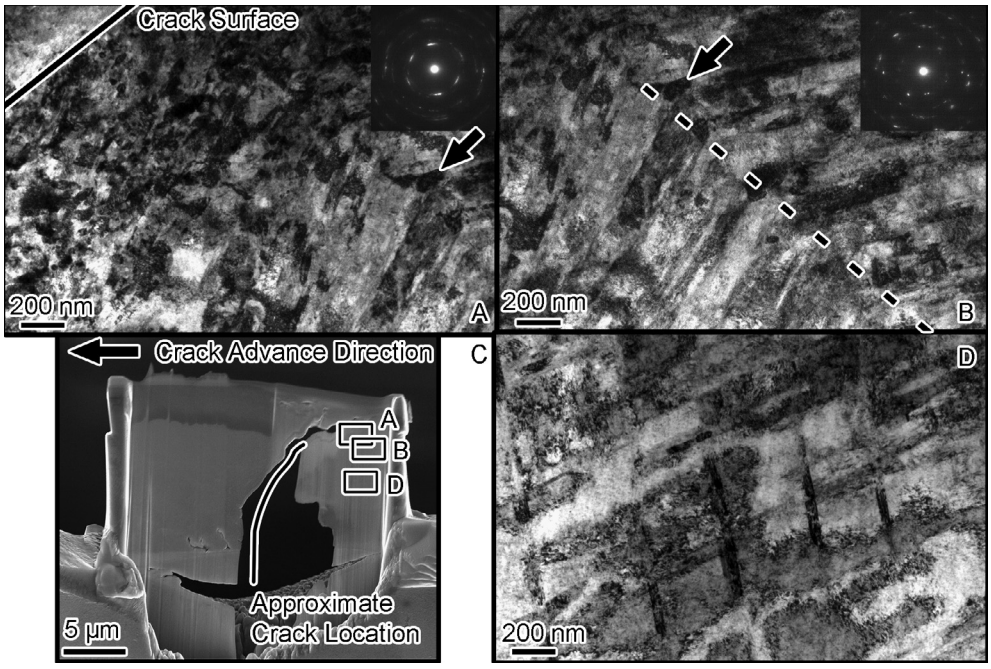

Fig. 13. Microstructure formed behind the crack as a function of distance. The position of the crack surface is indicated in (A). Arrow indicates common feature in (A) and (B). The change in orientation of the bands to correspond to a change in crack direction is highlighted by the white line.

revealed; the surface crack appears to lag behind the interior crack. Following the final thinning to electron transparency, there is loss of some of the sample behind the crack. The degree of loss of material is illustrated by the solid line in Fig. 11C, which is an approximate trace of the original crack position. Despite this loss most of cross-section has been preserved. The microstructure in the vicinity of the crack is compared as a function of distance from it in the micrographs presented in Figs. 12 and 13; the approximate position of each of the micrographs is shown in the SEM image that is included in each figure.

Both ahead and behind the crack tip there has been extensive refinement of the microstructure. Closer to the crack flank the microstructure is refined to the extent that subgrains a few hundred nanometers in size exist. Between these subgrains, as evidenced by the splitting of the diffraction spots presented as insets in Figs. 12A,B and 13A,B, small misorientations exist. With increasing distance from the crack tip and crack flanks the subgrain structure is replaced by a banded structure, Figs. 12D and 13B,D. The spacing between the bands is of the order of a few hundred nanometers and they change orientation to remain approximately parallel to the crack propagation direction. This is particularly evident in Fig. 13B, in which the lamellar structure can be seen to change direction without crossing a grain boundary; the change is highlighted by the addition of the dashed line. Further from the crack flank the microstructure becomes a simpler banded structure with similarities to the planar band structure seen in locations near to, but not at, the crack tip, Figs. 12D and 13D. Further ahead of the crack tip the sample shows shear banding with extensive dislocation activity.

The previous samples were all extracted from the sample surface ahead of the crack. To determine if refinement occurred in the interior of the sample, which would experience a different stress state than on the surface, samples were extracted normal to the fracture surface and in a region that exhibited striations on a second sample that was fatigued under the same conditions until final fracture occurred. Here, as shown in the fractograph presented in Fig. 14A, striations did not dominate the fracture surface. The location on the surface from which the sample was extracted is shown in Fig. 14B and the resulting microstructure in two different regions in Fig. 14C and D. Immediately beneath the striations exists a region that extends for about 200 nm that is comprised of fine subgrains, Fig. 14C and D. The subgrains, as indicated by the splitting of the spots in the diffraction pattern, are rotated by a few degrees with respect to each other; see diffraction pattern shown as the lower left inset in Fig. 14C. Beyond this region there exists a banded structure with an interband distance of a few hundred nanometers although this is variable. In this region the diffraction pattern shows no splitting of the diffraction spots; compare the diffraction patterns shown as insets in Fig. 14C. The interior of the bands contains a high dislocation density. On comparing the bands with the fracture surface there does appear to be some correspondence with the striation spacing although the correspondence is not one-to-one. The striation height and spacing is seen to be variable with small striations existing between the larger ones.

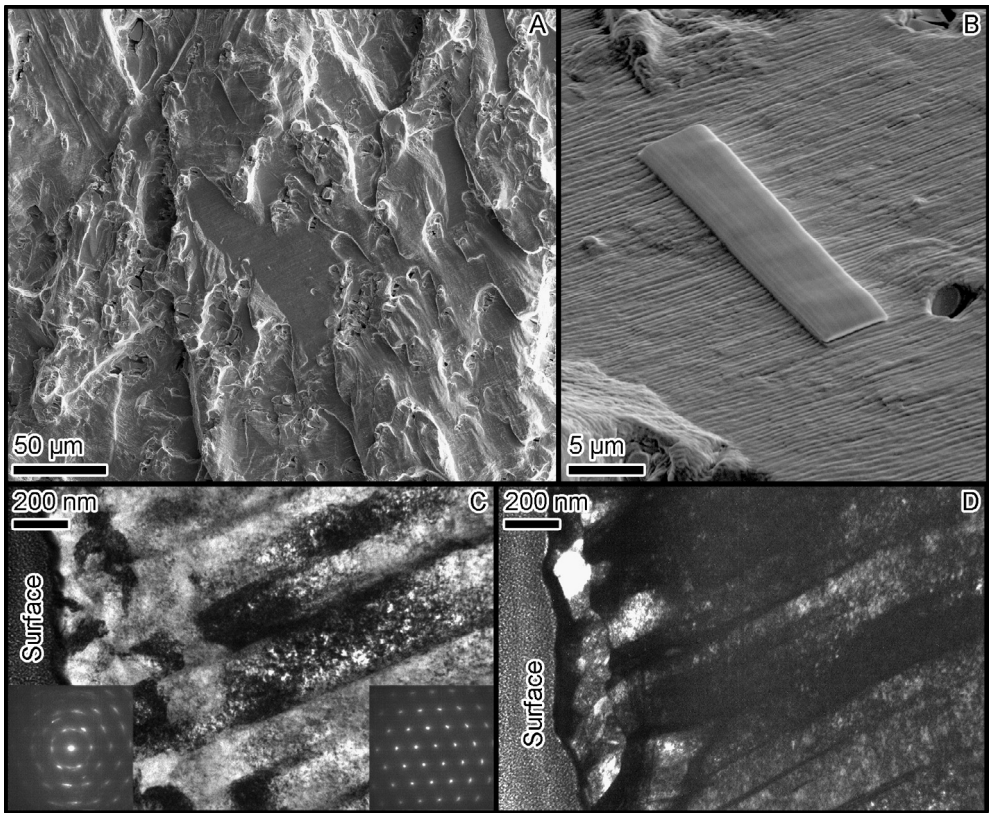

Fig. 14. Diffraction patterns, insets, are from the near-surface region, left pattern, and in the bulk, right pattern.

4. Discussion

The variation of the microstructure as a function of distance from a propagating crack interrupted after 53,355 cycles has been observed as a function of distance from the crack tip. It was found that as the crack is approached from a distance of some 800 μm, the microstructure evolves from simple planar slip with increasing dislocation content and a narrowing of the interband spacing to a microstructure exhibiting lamellar boundaries with a high dislocation content to a refined nanosized subgrain structure, typical of a material that has experienced significant and severe deformation [20]. The variation in the microstructure is more complex than the classical picture of dislocation arrangements in materials exhibiting planar slip behavior. That is, beneath the free surface the microstructure is not simply planar dislocation segments, dipoles and multipoles, which would be expected at low strain amplitudes, or dislocation tangles and loops as expected at high strain amplitudes. It was demonstrated that the planar features observed far from the crack tip can be correlated with the displacement on the free surface.

The microstructure observed in the vicinity of the crack exhibits characteristics, namely planar boundaries with an internal substructure, similar to those observed in stage IV monotonic loading with shear strains of unity [9,21]. As seen in Fig. 12A and B, a lamellar structure exists with an interboundary distance of the order of a few hundred nanometers. There is also a rotational difference between them as evidenced by the variation in the contrast. Within each lamella there is a substructure as evidenced by the local contrast fluctuations, which indicates these regions are rotated with respect to each other; this orientation difference is confirmed by the splitting of the diffraction pattern shown in the inset. Preliminary analysis by transmission EBSD of the misorientations between the lamellae shows rotational differences in excess of 5° [22]. This rotation, if substantiated by further analysis of additional boundaries, is significant in terms of the amount of strain that has occurred in this region. Such an evolved microstructure has also been observed to exist in 316 stainless steel that was subjected to fatigue loading (R-ratio $= -1$) although this structure formed beneath the fracture surface [23].

This study has shown the evolved microstructure ahead of an advancing crack consists of slip confined to planar bands away from the crack but shows more general deformation as the crack tip is approached. The far-field structure evolves well ahead of crack advance and this is the microstructure that the crack encounters as it propagates. The process of opening and closing the crack with each cycle and the concomitant increase in the local plastic strain must disrupt this microstructure and replace it with a graded structure that changes from ultrafine or nanoscaled

subgrains to a lamellae structure with increasing distance from the crack tip, Figs. 12 and 13. This evolution of the microstructure has important implications for considering how surface crack opening and closing processes operate and in dislocation-based modeling of those processes.

From the EBSD analysis, Fig. 4, it can be seen that there is an accumulation of strain at the grain boundaries within the plastic zone. The distribution of these strain concentrations occurs over a large distance and does not appear to be restricted to the extremes of the plastic zone. This increased plastic strain reflects the accumulation of dislocations at the grain boundary, consistent with them serving as barriers to dislocation slip and to the transmission of strain across the boundary. The distribution of strain along a grain boundary does not correspond necessarily to dislocation pileups spaced uniformly along the boundary, or to the existence of a dislocation structure along the boundary, but may reflect the accommodation of lattice dislocations in it and the mobility of the resultant dislocations along it. The microscopy that was conducted did not enable these possibilities to be distinguished. Nevertheless, grain boundaries do appear to have an influence on the propagation of slip. Blocking of a slip band associated with the crack has been used as the basis for assessing the threshold condition for propagation of a small fatigue crack [28]. The resulting model provided a lower bound of the threshold values of the stress required for slip to span the grains in terms of an associated local stress intensity factor. However, given the observations presented herein, it is interesting to ask if representing the material behavior in terms of slip transmission through a grain boundary is sufficient or if the determining microstructural length scale is associated with the complex high-strain microstructure observed in the vicinity of the crack.

The complex microstructure is also captured beneath striations on the fracture surface although the refined nanosized subgrain structure persists only to a depth of a few hundred nanometers before it is replaced with a banded structure containing a high density of dislocations. It is posited that the banded structure develops first and is replaced with the ultrafine subgrain structure in the process of crack advance in the formation of the striations. This refinement of the microstructure beneath fatigue striations is not unique to this system but has been reported to develop in 304 stainless steel fatigue tested (R-ratio $= -1$) in the presence of a high concentration of hydrogen, and in 316 stainless steel both in the presence and absence of hydrogen [23,24]. The lack of correlation between the striations and the substructure suggests striation formation may be associated with an accumulation of strain to a critical level rather than being associated with each cycle. It also confirms, as has been shown by slip models, that the concept of striation production via slip on two different slip systems is too simple [25,26]. Consequently, the models based, for example, on dislocation dynamics simulations do not capture the full complexity of the evolution of the microstructure during cyclic loading [27].

5. Conclusions

FIB machining has been used to extract samples normal to the surface ahead of a propagating stage II fatigue crack for subsequent TEM examination. This advance in sample preparation capability has provided new insights into the evolution of the microstructure as a function of the distance from the crack. Far from the crack, the microstructure could be predicted based on prior knowledge but the microstructure in the vicinity of the crack tip shows evidence of high levels of plastic strain that have not been reported previously. The observations suggest a re-evaluation of plasticity-based models of fatigue crack propagation. In addition, this refinement of the microstructure and the formation of the banded structures raise the interesting question of how striation markings originate on the fracture surface. For example, can the classical slip mechanism associated with striation formation form within such a refined microstructure? This is unlikely as the deformation must be confined to within one, or at most two, of the bands and these bands contain significant dislocation content prior to crack advance.

Acknowledgements

This work was supported by the US Department of Energy Nuclear Energy University Program (NEUP) under grant DOE-INL-000912. The electron microscopy was performed in the Center of Microanalysis of Materials in the Frederick Seitz Materials Research Laboratory at the University of Illinois.

References

[1] Chan KS. Int J Fatigue 2010;32:1428.
[2] Laird C. Fatigue. In: Robert WC, Peter H, editors. Physical metallurgy. Oxford: North-Holland; 1996. p. 2293 [chapter 27].
[3] Sangid MD. Int J Fatigue, in press, 2013, http://dx.doi.org/10.1016/j.ijfatigue.2012.10.009.
[4] Suresh S. Fatigue of materials. Cambridge: Cambridge University Press; 1998.
[5] Laird C, Charsley P, Mughrabi H. Mater Sci Eng 1986;81:433.
[6] Mughrabi H. Acta Metall 1983;31:1367.
[7] Mughrabi H, Ungár T. Long-range internal stresses in deformed single-phase materials: the composite model and its consequences. In: Nabarro FRN, Duesbery MS, editors. Dislocations in solids, vol. 11. Amsterdam: Elsevier; 2002. p. 343 [chapter 60].
[8] Li P, Li SX, Wang ZG, Zhang ZF. Prog Mater Sci 2011;56:328.
[9] Sauzay M, Kubin LP. Prog Mater Sci 2011;56:725.
[10] Wang ZR. Philos Mag 2004;84:351.
[11] Lukas P, Kunz L, Knesl Z, Weiss B, Stickler R. Mater Sci Eng 1985;70:91.
[12] Kayali ES, Plumtree A. Metall Trans A – Phys Metall Mater Sci 1982;13:1033.
[13] http://www.haynesint.com/230HaynesAlloy.htm. vol. 2013.
[14] Carroll JD, Abuzaid W, Lambros J, Sehitoglu H. Int J Fatigue, in press, 2013, http://dx.doi.org/10.1016/j.ijfatigue.2012.06.010.
[15] Robertson IM, Martin ML, Fenske JA. Influence of hydrogen on the behavior of dislocations. In: Gaseous hydrogen embrittlement of materials in energy technologies. Mechanisms, modelling and future developments, vol. 2. Cambridge, England: Woodhouse Publishing Limited; 2012. p. 166.

[16] Martin ML, Somerday BP, Ritchie RO, Sofronis P, Robertson IM. Acta Mater 2012;60:2739.
[17] Martin ML, Robertson IM, Sofronis P. Acta Mater 2011;59:3680.
[18] Martin ML, Fenske JA, Liu GS, Sofronis P, Robertson IM. Acta Mater 2011;59:1601.
[19] Nagao A, Smith CD, Dadfarnia M, Sofronis P, Robertson IM. Acta Mater 2012;60:5182.
[20] Hughes DA, Hansen N. Philos Mag 2003;83:3871.
[21] Hansen N, Huang X, Pantleon W, Winther G. Philos Mag 2006;86:3981.
[22] Keller RR, Geiss RH. J Microsc 2012;245:245.
[23] Martin ML, Auger T, Robertson IM, private communication, 2013.
[24] Martin ML, Sofronis P, Robertson IM, Awane T, Murakami Y. Int J Fatigue, in press, 2013, http://dx.doi.org/10.1016/j.ijfatigue.2012.08.009.
[25] Neumann P. Acta Metall 1974;22:1167.
[26] Neumann P. Acta Metall 1974;22:1155.
[27] Deshpande VS, Needleman A, Van der Giessen E. Acta Mater 2002;50:831.
[28] Tanaka K, Nakai Y, Yamahista M. Int J Fract 1981;17:519.